Electrochimica Acta 348 (2020) 136302

Contents lists available at ScienceDirect

Electrochimica Acta

journal homepage: www.elsevier.com/locate/electacta

Electrochemical fabrication of IrO_x nanoarrays with tunable length and morphology for solid polymer electrolyte water electrolysis

Zhuo-Xin Lu [a, d, e, f], Yan Shi [a, d, e, f, *], Pralhad Gupta [a], Xiang-ping Min [a], Hong-yi Tan [a, d, e], Zhi-Da Wang [a, d, e], Chang-qing Guo [a, d, e], Zhi-qing Zou [b, f], Hui Yang [b], Sanjeev Mukerjee [c], Chang-Feng Yan [a, d, e, f, **]

[a] Guangzhou Institute of Energy Conversion, Chinese Academy of Sciences, Guangzhou, 510640, PR China
[b] Shanghai Advanced Research Institute, Chinese Academy of Sciences, Shanghai, 201210, China
[c] Northeastern University, Dept Chem & Biol Chem, Boston, MA, 02115, USA
[d] Guangdong Provincial Key Laboratory of New and Renewable Energy Research and Development, Guangzhou, 510640, PR China
[e] Key Laboratory of Renewable Energy, Chinese Academy of Sciences, Guangzhou, 510640, PR China
[f] Dalian National Laboratory for Clean Energy, Dalian, 116023, PR China

ARTICLE INFO

Article history:
Received 6 February 2020
Received in revised form
14 April 2020
Accepted 22 April 2020
Available online 23 April 2020

Keywords:
IrO_x nanotube arrays
Controlled deposition
OER
MEA
PEM water Electrolysis

ABSTRACT

For a typical Proton exchange membrane (PEM) water electrolysis system, reducing the amount of Ir loading at the anode in membrane electrode assembly (MEA), while maintaining the performance, is still a big challenge. Here, to improve the performance of catalyst layer for oxygen evolution reaction (OER) in an acidic medium, vertical aligned IrO_x nanoarrays (IrO_x NAs) were synthesized by electrodeposition with TiO_2 nanotube arrays (TNTA) as template. By tuning the scan rate in the electrodeposition process, IrO_x open-end nanotube arrays with tunable length ranged from 500 nm to 1400 nm and hollow nanorod arrays were obtained due to a diffusion-controlled deposition process. By constructing 3-D electrode of 1-D catalyst with enhanced ion transfer, IrO_x NAs performed almost the same current density of OER with 1/20 Ir loading amount compared with commercial IrO_2 nanoparticles, which could significantly reduce the cost of catalyst in PEM water electrolyser. Moreover, no apparent current decrease was observed even after 10 h' anodic polarization under 1.55 V, which exhibit excellent OER durability.

1. Introduction

Electricity generated from intermittent renewable energy, such as solar and wind power, requires an appropriate storage system or medium to meet the requirements of power gird. In the past few years, several electrochemical energy conversion technologies have caught the attention of researchers and scientists [1,2]. With PEM electrolysis technology, the abandoned power due to the intermittent characteristics of renewable energy can be converted to hydrogen [3,4]. However, till now, PEM water electrolysis has not yet been extensively deployed in the commercial markets due to high associated costs. One of the driving factors for high costs of PEM water electrolysis is the use of highly rare and expensive precious noble metals as catalyst [5,6]. To reduce the cost, many efforts have been devoted to develop non-noble metal OER catalyst [7–9]. Unfortunately, lots of the materials were designed for OER in base condition, and the feasibility of these OER catalysts in acidic media is unknown. In the anode of PEM water electrolyzer, owing to the harsh condition in OER of PEM water electrolysis, Iridium is still irreplaceable considering of both activity and stability [10,11]. Moreover, the loading of Iridium in anode is significantly higher than noble metal in cathode due to the sluggish OER kinetics and stability issue. Hence, reducing the loading amount of precious Ir, while maintaining substantially higher activity and optimal stability, is of great concern [12,13].

One-dimensional nanoarrays electrode, which shows prominent properties in high utilization of catalyst, enhanced electron transfer and mass transfer, is considered as a promising solution to

* Corresponding author. Guangzhou Institute of Energy Conversion, Chinese Academy of Sciences, Guangzhou, 510640, PR China.
** Corresponding author. Guangdong Provincial Key Laboratory of New and Renewable Energy Research and Development, Guangzhou, 510640, PR China.
E-mail addresses: shiyan@ms.giec.ac.cn (Y. Shi), yancf@ms.giec.ac.cn (C.-F. Yan).

https://doi.org/10.1016/j.electacta.2020.136302
0013-4686/

achieve highly active electrode with low loading amount of catalyst [14–19]. It can be prepared with suitable one-dimensional nanoarrays, like carbon nanotube arrays and TiO_2 nanotube arrays, as a substrate or removable template. Pt/CNT arrays have been proven to be a highly active electrode for a membrane electrode assembly (MEA) in the fuel cell with substantially reduced Pt loadings [20,21]. However, under the high potential of OER, carbon could be easily corroded. By contrast, TiO_2 [22–26] and SnO_2 [27–29] with modification to improve its conductivity have been widely applied as supports for electrocatalyst. We synthesized partially reduced TNTA as support for IrO_x to fabricate an electrode with highly ordered arrays structure for OER [30,31]. In spite of the significant increment in the conductivity of the support, the thick oxide barriers formed at the bottom of the TNTA limited the improvement of the activity. Thus, to fabricate self-supported one-dimensional IrO_x NAs with removable template is more promising. Zhao et al. [32] had prepared 500 nm long IrO_x nanotube arrays with ZnO nanorod arrays as a removable template and the obtained catalyst showed 2.7 times higher turnover frequency than that of commercial IrO_2 nanoparticle in OER. Mafakheri [33] had applied Au-coated polycarbonate as a template to synthesize IrO_x nanotube arrays as an electrochemical sensor for Chromium and Arsenic. TNTA, which presents much higher-ordered orientation and distribution than ZnO nanorod arrays and polycarbonate, is a rational candidate for removable template to prepare 1-D nanoarrays as well. Cerro-Lopez et al. [34] studied the process of electrodepositing PbO_2 onto TNTA in galvanostatic method, in which PbO_2 deposited evenly on the whole nanotube at the first few seconds and then started to form a cover layer on the top surface of TNTA. To avoid the formation of the cover layer and achieve a controllable 1-D structure, bottom-up deposition and pulse deposition on TNTA has been widely studied. For bottom-up deposition, Macak et al. [35] prepared TNTAs with higher conductivity of the bottom by controlled doping treatment. With a controlled polarization time of 2–5 s, only the bottom of nanotube was doped which displayed higher conductivity than the tube wall, which made the bottom-up electrodeposition of copper possible and finally formed solid copper nanorods. Wang et al. [36] reported an approach of complete filling semiconductor in TNTA. This study underlined bottom-up or top-overlaying deposition by adjusting the ambipolar diffusion length of electron and ion by changing the solvent composition and precursor concentration of electrolyte. For pulse deposition, Sang et al. have achieved evenly depositing of Cu on TNTA with pulse time of 0.1s and relaxation time of 0.3s. However, both bottom-up deposition and pulsed deposition lead to end-block layer at the bottom of TiO_2 nanotube. As the catalyst layer on the tube wall of TNTA is required to be an open-end and continuous tube to form a self-supported nanoarrays with optimum utilization of catalyst surface, the main challenge is to deposit continuous catalyst layer at the upper part of nanotube without forming a compact cover layer.

In this study, a cyclic voltammetry (CV) deposition method was applied for depositing IrO_x into TNTA. Different from the previous reports, the deposition of IrO_x nanotube arrays with tunable length has been achieved successfully without any modification of TNTA. Meanwhile, the as-prepared IrO_x NAs could be controlled as two morphologies, open-end nanotube arrays (NTs) and hollow nanorod arrays (NRs). The synthesis method and the possible mechanism of controlled deposition have also been presented in this study. In order to investigate the performance of such vertical aligned nanotube arrays on OER, IrO_x NAs were transferred onto Nafion membrane and tested in a half cell electrochemical system. Various electrochemical characterization techniques, including CV, LSV and EIS were used for testing the performance and stability under OER potential.

2. Experiment

2.1. Preparation of IrO_x NAs

The vertically aligned IrO_x NAs were prepared by adopting 3 major steps: (1) electrodeposition, (2) transferring, and (3) template removal step as Fig. 1 shows. Titanium foils (35 mm × 10 mm × 0.1 mm) were degreased by ultrasonic treatment in ethanol and deionized water and were used to synthesize TNTA with by anodizing in 0.4 mol/L NaF solution with an applied potential of 15 V for 1 h. After calcining at 623 K for 1 h, TNTA was applied as a working electrode for electrochemical deposition of IrO_x by CV method with different scan rates ranging from 20 mV/s to 150 mV/s. The range of CV scan was from 0.2 V to 1.0 V (vs. RHE) with graphite rod and Ag/AgCl electrode used as counter electrode and reference electrode, respectively. The Ir precursor was prepared as reported previously [30].

Before attaching to Nafion membrane, Nafion ionomer was coated on to IrO_x by dropping 10 μl of 0.05 wt% Nafion solution, followed by drying under an infrared lamp. This step was consecutively repeated for 5 times, and then the sample was dried at 353 K under vacuum.

Then IrO_x@TNTA was hot-pressed onto the Nafion membrane at the temperature of 413 K and pressure of 4 MPa for 90s. After that, a two-step etching was conducted to remove the template by etching in 0.2%wt and 20%wt HF successively to obtain IrO_x NAs, which is crucial to obtain a catalyst layer of IrO_x NAs by avoiding the damage caused by hydrogen generated during the removal of metal titanium.

2.2. Characterization

The morphology of as-prepared samples was observed by scanning electron microscope (SEM, Hitachi S4800). Transmission electron microscope (TEM, JEM-2100 F) is used to study morphology and crystal structure. The chemical state of IrO_x NAs was analyzed by X-ray photoelectron spectroscopy (XPS, ESCALAB 250Xi spectrometer with Mg Kα source with hv = 1253.6 eV under vacuum). The loading amount of IrO_x NAs on the Nafion membrane was measured by X-ray fluorescence (XRF, AXIOSmAX-PETRO, PANalytical B·V.) with 0.1 mg Pt as internal standard.

2.3. Electrochemical analysis

The electrochemical test of performance of OER in ultrapure water was carried out with a three-electrode system in self-made half-cell (Fig. S1). All the electrochemical measurements were performed with CHI660 electrochemical workstation in three-electrode system, in which Pt coated Ti foil was used as a counter electrode and Hg/Hg_2SO_4 electrode was used as a reference electrode. A porous Ti plate with the surface area of 1 cm^2 is used as a current collector. The Nafion membrane across the reference chamber and reacting chamber act as a salt bridge.

3. Result and discussion

3.1. Electrodeposition of IrO_x on TNTA

The electrodeposition of IrO_x was conducted by cyclic voltammetry scan ranged from 0.2 V to 1.0 V with Ir precursor of $[Ir(COO)_2(OH)_4]^{2-}$ (Fig. 2a). The deposition reaction occurs at positive scanning with potential above 0.8 V by oxidizing the oxalic acid ligand and release CO_2 as given by the equation below [37,38]. The redox peak at around 0.65 V can be attributed to the transformation of Ir^{IV}/Ir^{V}, which represent the electrochemical surface area of IrO_x.

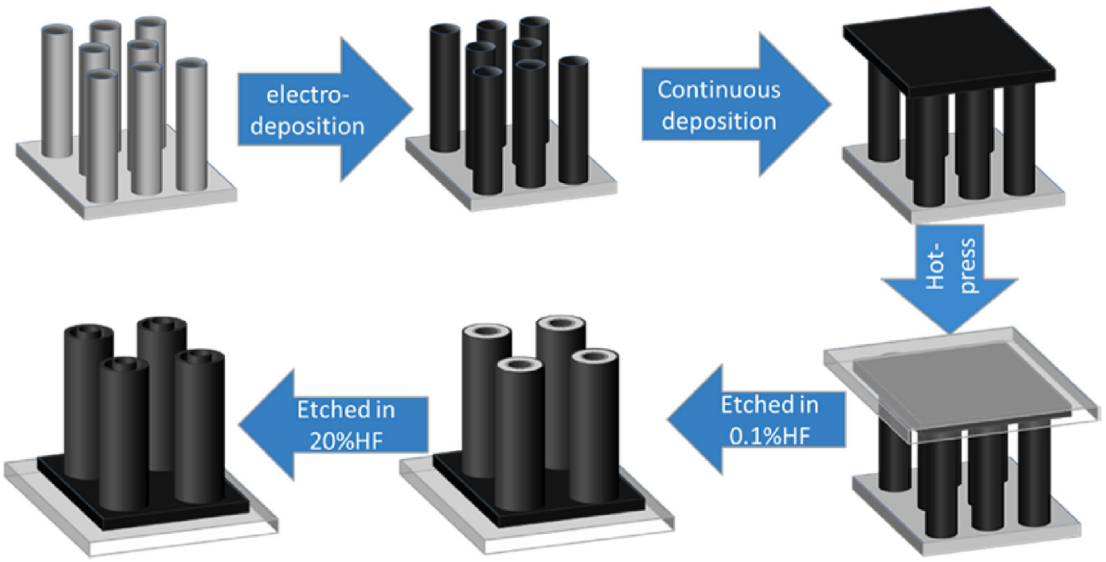

Fig. 1. Scheme for the preparation strategy for IrO_x NAs.

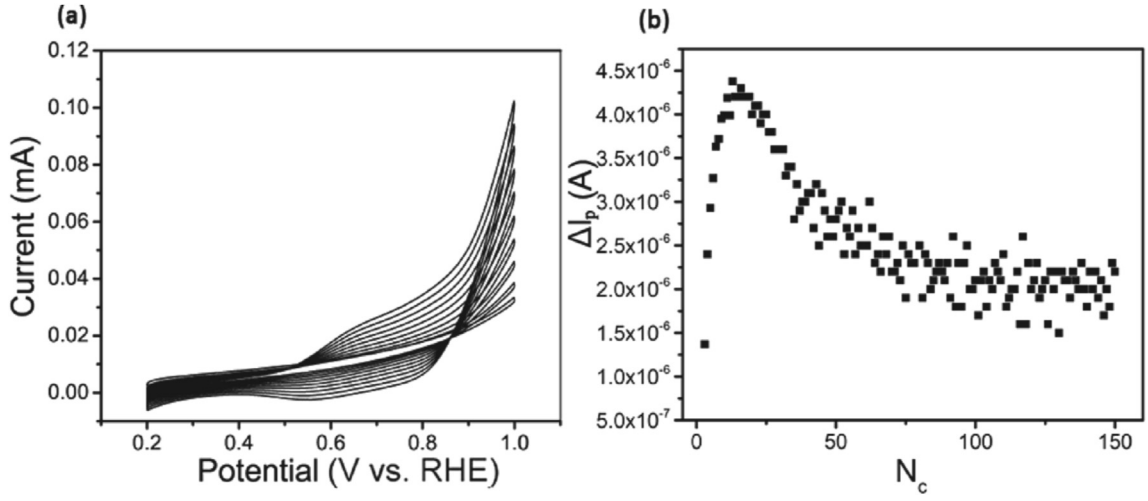

Fig. 2. (a) CV curve of IrO_x depositing on TNTA with a scan rate of 20 mV/s, (b) The relationship between the increment of peak current at 1.0 V (ΔI_p) and numbers of depositing cycles (N_c).

$$[Ir(COO)_2(OH)_4]^{2-} \rightarrow IrO_x + 2CO_2 + 2H_2O + 2e^- \quad (1)$$

During the electrodeposition process, the current in Fig. 2a was found to be smoothly increasing with the increasing number of deposition cycles, which indicates the continuous formation of IrO_x. To obtain a further insight of the depositing process, the variation of increment of peak current at 1.0 V (ΔI_p) in positive scan with the numbers of cycles (N_c) is studied (Fig. 2b). In the first few cycles, the current increases quickly with the increase in the number of cycles. As the deposition continues, with the increasing amount of the nucleus of IrO_x, particle growth becomes dominant gradually and results in increasing ΔI_p. After the peak value of ΔI_p is reached, it gradually starts decreasing. It is probably due to two following reasons: 1) active surface area decreases due to the formation of a dense layer of IrO_x from isolated particle; 2) loss of accessible IrO_x surface for deposition inside the nanotube due to the gradually shut down of the tube's mouth arising from IrO_x deposition.

When the deposition keeps on proceeding, the curve of N_c-ΔI_p reaches a plain averagely, which indicates the formation of a cover layer of IrO_x on the top surface of TNTA. The cover layer hinders the diffusion of Ir precursors form the bulk electrolyte to the tube wall and further results in a preferential deposition on the cover layer. It can be verified by the fact that the length of IrO_x nanotube prepared at the scan rate of 20 mV/s with 50, 100 and 150 cycles were similar. By contrast, cover layers with thickness of 103 nm and 155 nm were presented when exceeding numbers of depositing cycles were applied (Fig. 3). Therefore, it is unlikely to obtain longer IrO_x NAs just by increasing the number of cycles.

3.2. Length control of IrO_x NAs

The electrodeposition of IrO_x is a diffusion-controlled process [39]. The study of electrodeposition in anodic alumina oxide (AAO) reported by Graf [40] shows that, with continuous depositing, the precursor concentration at the bottom of nanotube decreased as the length of AAO increased. It is suggested that a concentration gradient along the nanotube can be formed with continuous deposition and the electrodeposition in nanotube is a diffusion-

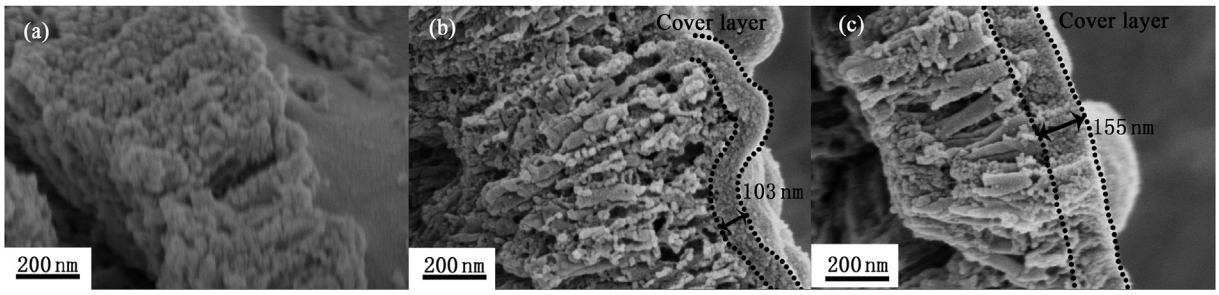

Fig. 3. The SEM image of IrO_x NAs synthesized by deposition at the scan rate of 20 mV/s with 50 cycles (a), 100 cycles (b) and 150 cycles (c) that performs similar length with different thickness of cover layer.

controlled process. In our study, unlike AAO, the whole nanotube of TNTA is electrically conductive. Electrodeposition was observed at the mouth, bottom, and the wall of TiO_2 nanotube, which enhances the consumption of precursor along the nanotube. Therefore, to improve the inner deposition of nanotubes, the concentration distribution of Ir precursor inside the tubes plays a crucial role. By varying the scan rate of CV during the deposition process, the duration time of Ir deposition and relaxation time for the rebuilding of the precursor can be tuned, and this would affect the concentration and distribution of Ir precursor along the nanotube. To investigate the morphology control of IrO_x NAs with CV electrodeposition, IrO_x NAs synthesized with various scan rates were studied (Fig. S2). IrO_x NAs in Fig. 4 clearly show the different length which prepared by altering scan rate in CV deposition process. At a relatively slow scan rate of 50 mV/s, IrO_x nanotubes with length of approximately 550 nm were obtained (Fig. 4a). Furthermore, as the scan rate increased, for example at the scan rate of 70 mV/s, the length of the nanotubes increased to 1100 nm (Fig. 4b). Moreover, the further increase in the scan rate to 80 mV/s or above, the length of the IrO_x NAs stretched to over 1400 nm, which reaches to the maximum as it equals to TNTA template (Fig. 4c). Fig. 5 displays the relationship between the scan rate and the length of the IrO_x NAs, in which three stages are presented. With the precursor concentration of 1.3 mg_{Ir}/ml and the scan rate below 50 mV/s, nanotubes with the length around 500 nm can be obtained. Further increase the scan rate to 80mv/s, the length of nanotubes was found increasing almost linearly with the scan rate until it reaches to the maximum. This suggests a scan rate dependence in the length control of IrO_x NAs by CV deposition method.

The result above can be explained by the electrodeposition process on the inner wall of the tube (Fig. 6). At the beginning of the deposition, when the applied potential was lower than the oxidizing potential of oxalic acid ligand, the precursor was homogeneously distributed in the TNTA. At the start of the deposition process, only a small amount of IrO_x particles were averagely deposited on the entire nanotube. Along with the continuation of the deposition, there was a rapid decrease in the concentration of Ir beneath the mouth of the TNTA and concentration gradient, which decrease from the mouth to the end of TNTA, formed as the simultaneous effect of diffusion and deposition. Consequently, uneven deposition along the nanotube occurred and the deposition at the depth of nanotube, where the supply of Ir precursor form bulk electrolyte cannot reach, was terminated. In contrast, at the mouth of the nanotube, the deposition proceeded constantly with sufficient diffusion and eventually formed a cover layer of IrO_x on the mouth of TNTA as described in 3.1. In a nutshell, for the electrodeposition process in each cycle, both even and uneven depositions are involved along the TNTA. However, the extent of evenness is characterized by the duration of continuous deposition, which in turn is determined by the scan rate as pointed out in this study.

Thus, the slower scan rate exhibits an extended duration of IrO_x deposition, which exhausts the precursor inside the nanotube even before the deposition of single cycle ends and results in preferential deposition at the mouth of the nanotube. And longer duration of IrO_x deposition in a single cycle leads to the formation of cover layer within fewer number of depositing cycles. In addition, the insufficient nucleation sites prohibit the formation of a continuous layer of deposited IrO_x particles at the inner wall of the nanotube before the mouths of TNTA are blocked. Thus, only short IrO_x nanotube are formed near the mouth of the TNTA. Unlike lower scan rate, at a substantially higher scan rate, the deposition time in each cycle is relatively short, which requires comparatively a larger number of cycles to form the cover layer at the tube's mouth. Henceforth, it facilitates the mobility of Ir precursor into the nanotube and allows an improved inner deposition. Therefore, higher scan rate leads to more uniform deposition and longer continuous nanotubes.

The controlled deposition with a lower concentration of Ir precursors advances in relevance to the aforementioned study and presents a linear region between the scan rate of deposition and length of IrO_x NAs. As shown in Fig. 5b and c, we can see that, with lower concentration of precursor i.e. 0.65 mg_{Ir}/ml and 0.26 mg_{Ir}/ml,

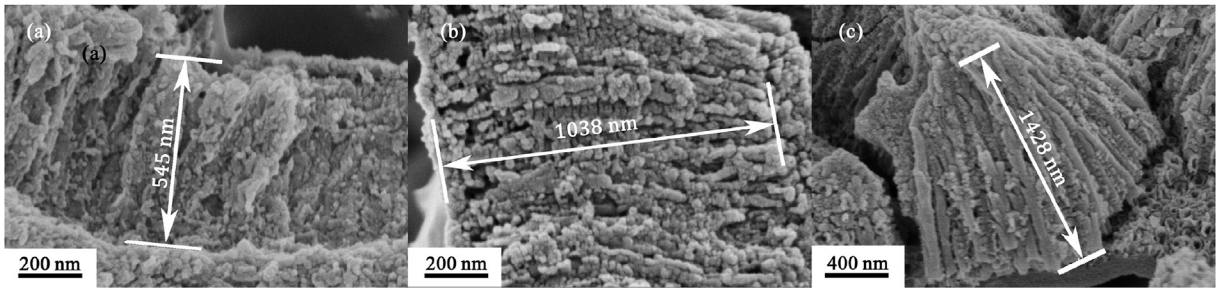

Fig. 4. The SEM image of IrO_x NAs with different length prepared at different scan rate of 50 mV/s (a), 70 mV/s (b) and 80 mV/s (c).

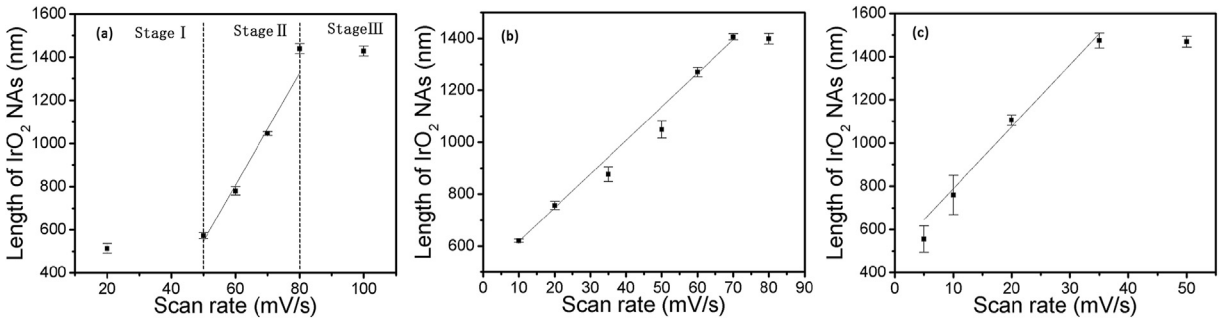

Fig. 5. The relationship between the length of IrO_x NAs and a scan rate of IrO_x deposition on TNTA with different concentration of Ir precursor of 1.3 mg_{Ir}/ml (a), 0.65 mg_{Ir}/ml (b) and 0.26 mg_{Ir}/ml (c).

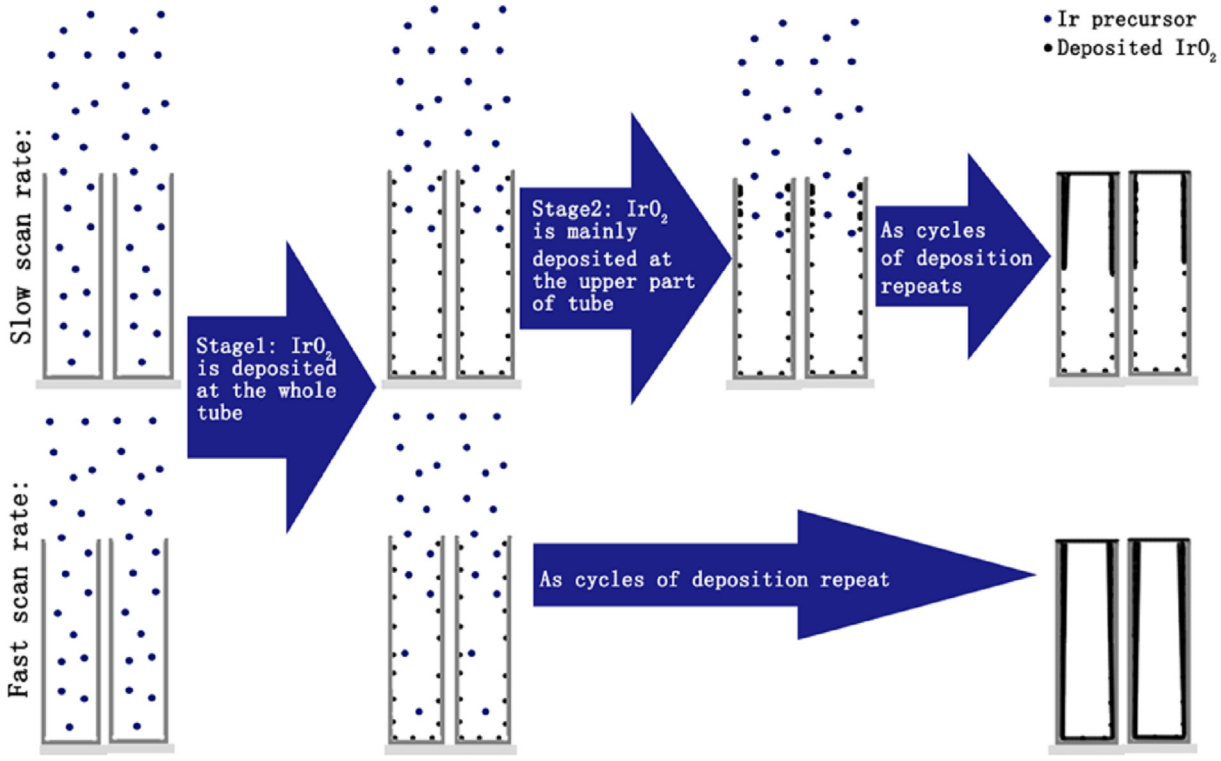

Fig. 6. Scheme of depositing model controlled by scan rate of CV.

the linear stage shifts to the lower scan rate, and longer nanotubes can be obtained at the same scan rate value. It signifies that due to the lower concentration of precursor, the deposition rate at the mouth of the TNTA reduces, which in turn requires more cycles to form the covering layer. This enables the optimum transport of Ir precursor, fashioning the uniform deposition along the nanotubes.

It can be noted that the deposition of IrO_x on the TNTA can be divided into two different part depending upon the trend of depositing rate as the deposition goes on. The deposition at the mouth of the TNTA remains constant due to sufficient diffusion, which is determined by the total depositing time and depositing rate. However, the uniform deposition of IrO_x on the tube wall is mainly determined by the total number of depositing cycles prior to the formation of a cover layer. Furthermore, it can be presumed that by employing a longer template, longer IrO_x NAs can be obtained by further increasing the scan rate.

3.3. *Characterization of IrO_x nanoarrays*

As can be seen from SEM images, the obtained IrO_x NAs consisted of nanotube surrounded by porous nanotube (Fig. 7a) or one-dimensional hollow nanorod (Fig. 7b). In order to identify the chemical composition of IrO_x NAs, EDS was implemented as shown in Fig. 7c. The results indicate that the obtained nanoarrays is pure IrO_x and the template has been completely removed. The trace signal of titanium is supposed to be residual titanium ion absorbed at the surface of IrO_x NAs after the etching treatment. The signals of F element shown in the EDS data may arising from the F in perfluoro sulfonic acid ionomer such as Nafion sprayed on IrO_x NAs. Unlike the study performed by Macak [35] and Wang [36] which emphasized on solid nanorod arrays by bottom-up deposition with the modification of TNTA or electrolyte, our study encompassed the deposition of the entire nanotube without any modification of the TNTA. Consequently, nanotube or hollow nanorod structure were

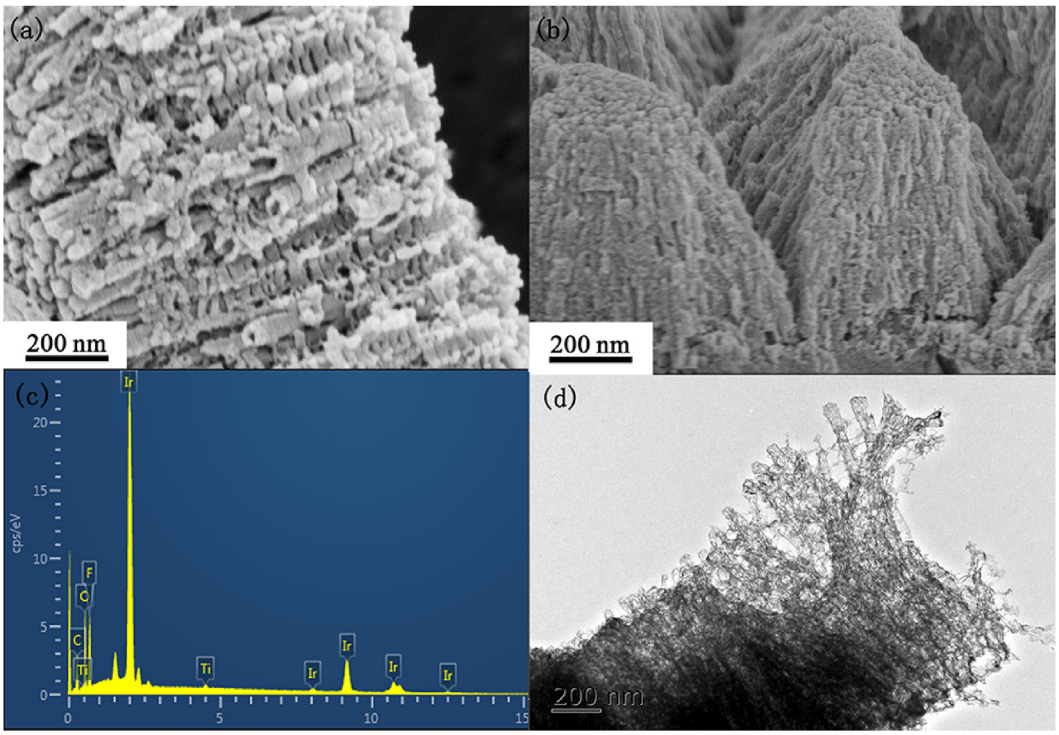

Fig. 7. The morphology of IrO_x nanotube arrays (a) and IrO_x hollow nanorod arrays (b); EDS of IrO_x NAs (c) and TEM (f) image of IrO_x nanotube arrays (d).

obtained in this study. The hollow nanorod or nanotube with an average outer diameter of 60 nm was found consistent with IrO_x deposited on the inner tube wall of TNTA, while the porous structure was observed to be IrO_x deposited on the outer tube wall of TNTA. As there were ribs that partly connected adjacent tubes on the outer tube wall of TNTA (Fig. S3b), IrO_x could not form a completely continuous layer along the entire outer tube, which resulted in the formation of porous nanotubes. Fig. 7b shows that IrO_x NAs with larger aspect ratio were found to be accumulated. This phenomenon was also observed in the study of Pd—Fe nanorod reported by Nevin [41]. By transmission electron microscopy (TEM), the outer diameter of the nanotube was found to be approximately 57 nm, which ratified the inner diameter of the TNTA (Fig. 7d).

The chemical state of Ir in Ir oxides is very crucial to OER performance. Recent studies [10,42] indicated that Ir in lower oxidation state such as Ir^{3+} can be used as an ex-situ descriptor for OER activity prediction. In-situ XAS studies revealed that Ir^{3+} species can transform to higher valence of Ir species under oxidation potential, and then active O species (O^-) will form to maintain the charge balance. These active O species can facilitate the formation of O—O bond and speed up OER kinetics [43]. In view of this, X-ray photoelectron spectroscopy (XPS) was used to investigate the chemical state of IrO_x NAs. As shown in Fig. 8a, in the spectrum of Ir, two peaks around 62.5 eV and 65.5 eV are corresponding to $Ir4f_{5/2}$ and $Ir4f_{7/2}$ of Ir^{3+}, while the peaks at 63.4 eV and 66.3 eV are assigned to Ir^{4+}. The result suggests that Ir species in IrO_x prepared by electrochemical deposition mainly exists in form of Ir3+, which is consistent to our previous study [30].

The spectrum of O1s core level is measured to investigate the chemical state of O species of IrO_x. Considering the absence of Ti signals in XPS spectra (Fig. S6), the O signals in the O1s spectra must be related to the O species in Ir oxides and Nafion ionomer. In Fig. 8b, three main peaks are characterized. The peak around 530 eV and 532 eV are assigned to lattice O in oxide and —OH group, respectively, while the peak at 533.5 eV corresponds to the absorbed water. Also, there is a weak peak centered at 534 eV, which can be assigned to the O species of Nafion [44,45]. This suggests the little contribution of Nafion on O 1s spectra and the strong peak around 532 eV is mainly due to the large amount of Ir—OH on the surface of nanoarrays, which is consistent to the dominated Ir^{3+} for Ir species. Such high concentration of —OH group is in line with the results of Ir oxides prepared by electrochemical deposition method, and it is also an indication of high OER activity [46].

3.4. Electrochemical performance of IrO_x nanoarrays

The electrochemical performance of IrO_x NAs with different morphology were studied in home-made half-cell. The CV curve of different IrO_x NAs with a scan rate of 100 mV/s are presented in Fig. 9a. There are two pairs of redox peaks around 0.9 V and 1.3 V, which correspond to the transformation of Ir^{III}/Ir^{IV} and Ir^{IV}/Ir^{V}, respectively. The area in CV curves can be used to reflect the electrochemical surface area of catalyst. It can be observed that larger electrochemical active surface area (ECSA) was observed with the increasing length of IrO_x nanotube. For the sample with hollow nanorod structure, lower capacitance current was found compared to a nanotube structure, which can be ascribed to the inaccessible inner surface of nanotubes due to the sealed tube mouth. Henceforth, the open-end nanotube structure is expected more favorable for achieving higher utilization of catalyst in a one-dimensional structure.

The OER activity of as-synthesized IrO_x NAs is shown in Fig. 9b. Compared with the conventional catalyst layer prepared by spraying method with commercially IrO_x nanoparticles (loading amount: 3.8 mg_{Ir}/cm^2), IrO_x hollow nanorod arrays with a length of 500 nm (loading amount: 0.18 mg_{Ir}/cm^2) showed the comparable current density of OER with 20 times lower loading amount of IrO_x. This indicates a significant improvement of Ir mass activity with IrO_x nanotube arrays. Such high performance can be explained by

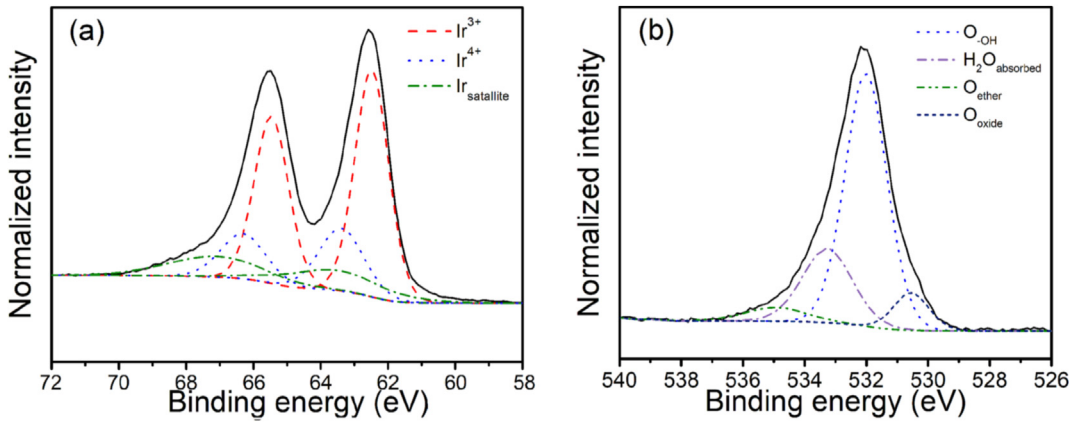

Fig. 8. The XPS spectrum of Ir 4f core level (a) and O 1s core level (b) of IrO_x NAs.

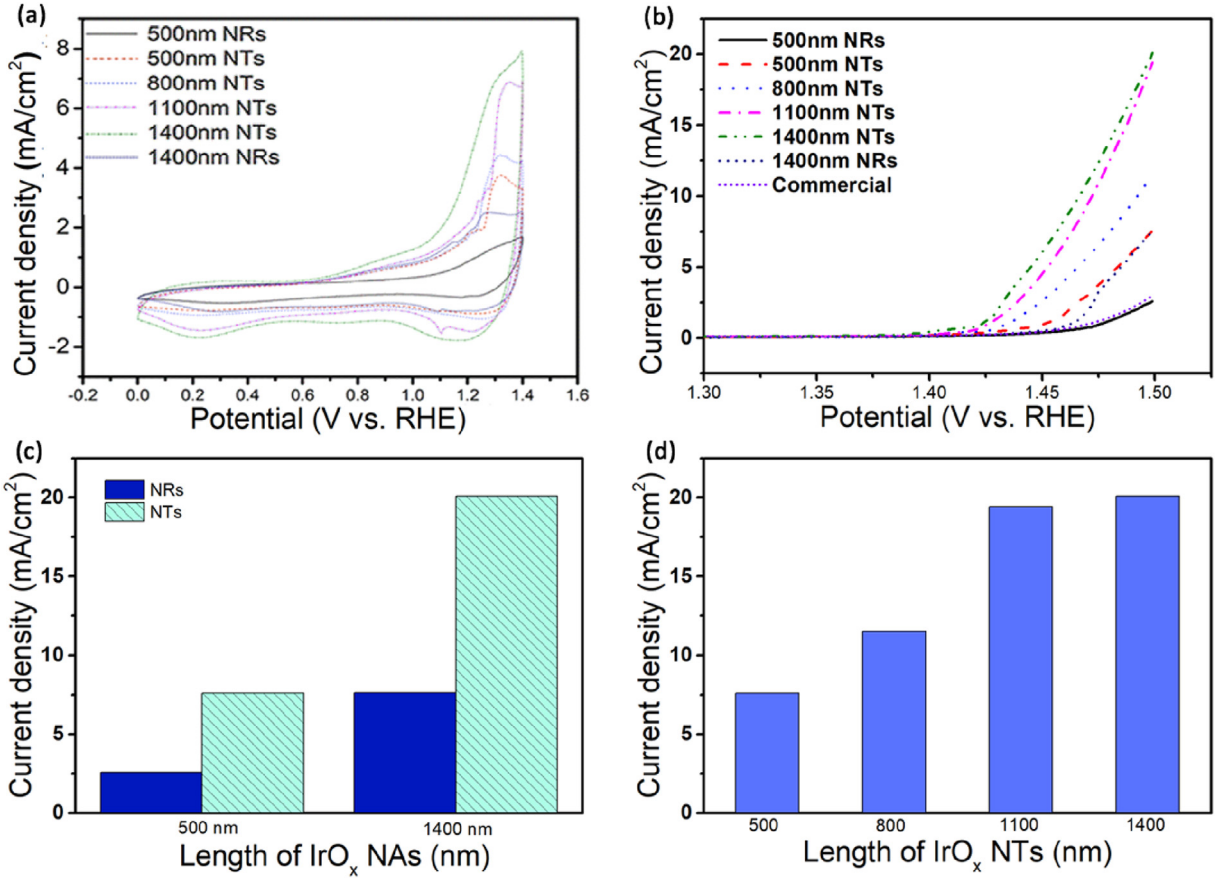

Fig. 9. CV tests of IrOx NAs under the scan rate of 100 mV/s(a); LSV tests of IrO_x NAs and commercial IrO_x nanoparticles under the scan rate of 1 mV/s (b); comparison of OER activity of IrO_x NAs with different morphology (c) and IrO_x nanotube with different length (d) at 1.5 V.

the higher activity of electrodeposited Ir oxides and highly ordered 1-D nanostructure. For nanotube arrays with open-end structure, the sample with length of 500 nm performs 7.16 mA/cm^2 at 1.5 V, which is 2.9 times and 2.4 times higher than that of nanorod arrays and commercial IrO_x nanoparticle. This result indicates a potential influence of morphology on OER activity. Similar result is also observed in the comparison of the samples with both length of 1400 nm but different morphology (Fig. 9c).

Fig. 9d depicts the influence of nanotube length on OER performance. The OER activity was found increases with the increasing of tube length. For the samples with length shorter than 1100 nm, the OER current increases almost linearly with tube length. While the length exceeds 1100 nm, the current tends to reach a constant value. Such limited OER current of the sample with longer tube can be explained by the restricted ECSA, which must be due to the lack of proton access to the active sites which located far from the membrane surface. In addition, the longer nanotube may also affect the mass transport in the catalyst layer such as oxygen gas evolution and water transport to the active sites.

As discussed above, IrO_x nanotube arrays with vertically aligned

structure exhibited remarkable enhancement of surface area and OER current than the conventional catalyst layer. In order to present the advantage of such vertically aligned and continuous tubes, the complex capacitance of nanoarrays and conventional catalyst layer measured by EIS method and presented. The EIS plot has been demonstrated as a useful tool for studying the porous electrode [47], and the complex capacitance can be easily transformed from Nyquist plots. Capacitance and impendence can be correlated with each other as shown below:

$$C'(\omega) = \frac{-Z''(\omega)}{\omega|Z(\omega)|^2} \quad (2)$$

$$C''(\omega) = \frac{Z'(\omega)}{\omega|Z(\omega)|^2} \quad (3)$$

$C'(\omega)$ is the real part of the complex capacitance. From the plot of $C'(\omega)$ vs. frequency, the total capacitance of the electrode can be calculated by extrapolating at extremely low frequency. $C''(\omega)$ is defined as the imaginary part [48]. From this complex capacitance plot, relaxation time, which reflects the migration of ions in the electrode can be obtained. In Fig. 10, the $C''(\omega)$ of all the IrO_x NAs sample exhibit maximum at certain frequency (f) respectively, and the corresponding relaxation time constant equals to be $1/f$. The IrO_x nanotube arrays shows the relaxation time range from 1.47 to 5.62 s. In contrast, the $C''(\omega)$ of the conventional catalyst layer does not show a peak in frequency range applied in the test. Henceforth, it is obvious that IrO_x nanotube arrays showed a shorter relaxation time, suggesting the lower resistance of ion transport [49].

To assess the OER stability, potentiostatic test at 1.55 V vs. RHE was applied in home-made half-cell for 10 h, and the current retention at 1.5 V was used to evaluate the stability. During stability test, a typical i-t curve was observed in Fig. S7. The relative stable OER current with time indicates the stability of as-prepared sample. The current retention of different samples after 10 h anodic polarization are all above 90% (Fig. 11), suggesting the excellent durability. This is very different to the stability results of such electrodeposited IrO_x. According to previous reports [50], IrO_x prepared by anodic electrodeposition method always show higher performance but poor OER stability. In the present work, the electrodeposited IrO_x, however, exhibit unexpected stability. Such results may be explained by the unique structure of nanotubes which can mitigate the particle agglomeration, dissolution and stabilize the active surface area [51,52].

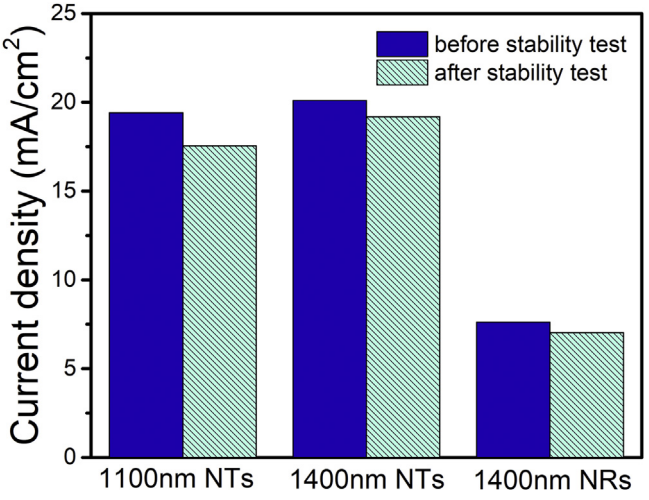

Fig. 11. Current retention of IrO_x NAs at 1.5 V after stability test.

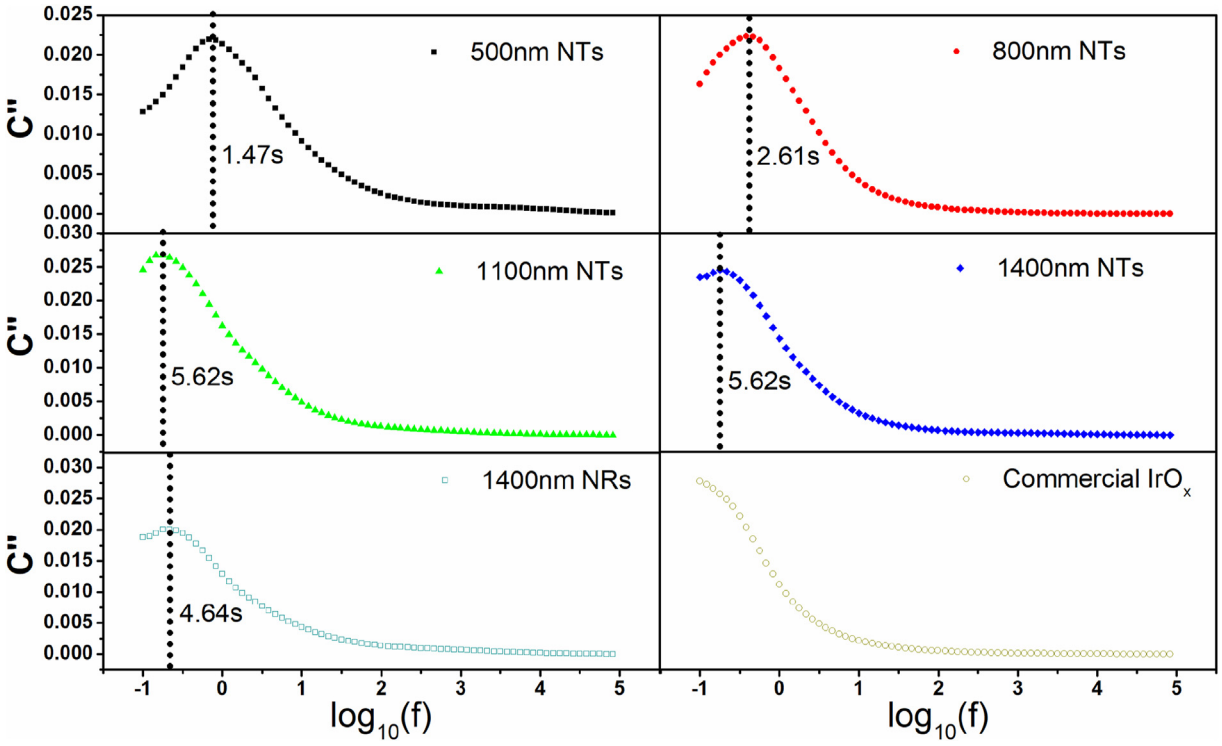

Fig. 10. The curve of imaginary capacitance – frequency of IrO_x NAs in 1 cm^2 half-cell testing for the calculation of relaxation time.

4. Conclusion

Using TNTA as a removable template, this study proposed a controlled electrodeposition method to synthesize open-end IrO_x nanotube arrays with the controllable length for the application in the anode catalyst layer of PEM water electrolysis. By applying different scan rate and concentration of Ir precursor, the length of IrO_x nanotube arrays was varied from about 500 nm to 1400 nm. The mechanism of tunable synthesis is characterized for utilizing the diffusion-controlled deposition along nanotube with the high aspect-ratio. The IrO_x nanotube arrays structure equipped with open-end can be an appropriate choice to prepare a catalyst coated membrane. The OER activity of IrO_x NAs@Nafion is correlated to the surface area of exposed IrO_x and revealed a prominent mass activity with enhanced ion transport compared to IrO_x nanoparticle. By using open-end 1-D nanotube arrays electrode, the requirement of current density can be met with much lower loading of the noble metal. And prominent stability of IrO_x NAs sample are shown, guaranteeing possibility of practical application as order electrode for MEA. Furthermore, it is possible to extend the tunable length of obtained nanoarrays to the order of millimeter by applying TNTA template with long length that prepared in ethylene glycol electrolyte.

Declaration of competing interest

The authors declare that they have no known competing financial interests or personal relationships that could have appeared to influence the work reported in this paper.

CRediT authorship contribution statement

Zhuo-Xin Lu: Methodology, Investigation, Writing - original draft. **Yan Shi:** Conceptualization, Methodology. **Pralhad Gupta:** Writing - review & editing. **Xiang-ping Min:** Validation. **Hong-yi Tan:** Investigation. **Zhi-Da Wang:** Formal analysis. **Chang-qing Guo:** Visualization. **Zhi-qing Zou:** Resources. **Hui Yang:** Resources. **Sanjeev Mukerjee:** Writing - review & editing. **Chang-Feng Yan:** Conceptualization, Supervision, Funding acquisition.

Acknowledgements

This work was financially supported by the National Natural Science Foundation of China (51576201), DNL Cooperation Fund, CAS (DNL180405), Natural Science Foundation of Guangdong Province (2015A030312007, 2017A030310539 and 2018A050506071), Guangzhou Science and Technology Project (201904010412).

Appendix A. Supplementary data

Supplementary data to this article can be found online at https://doi.org/10.1016/j.electacta.2020.136302.

References

[1] M. Goetz, J. Lefebvre, F. Moers, A.M. Koch, F. Graf, S. Bajohr, R. Reimert, T. Kolb, Renewable Power-to-Gas: a technological and economic review, Renew. Energy 85 (2016) 1371–1390.
[2] E. Troncoso, M. Newborough, Electrolysers for mitigating wind curtailment and producing 'green' merchant hydrogen, Int. J. Hydrogen Energy 36 (2011) 120–134.
[3] M. Zhou, Y. Liu, Ieee, Theoretical Study on Direct Coupling of a PV Array to a PEM Electrolyser, 2013.
[4] M. Ni, M.K.H. Leung, D.Y.C. Leung, Energy and exergy analysis of hydrogen production by a proton exchange membrane (PEM) electrolyzer plant, Energy Convers. Manag. 49 (2008) 2748–2756.
[5] Y. Li, X. Du, J. Huang, C. Wu, Y. Sun, G. Zou, C. Yang, J. Xiong, Recent progress on surface reconstruction of earth-abundant electrocatalysts for water oxidation, Small 15 (2019).
[6] X. Du, J. Huang, J. Zhang, Y. Yan, C. Wu, Y. Hu, C. Yan, T. Lei, W. Chen, C. Fan, J. Xiong, Modulating electronic structures of inorganic nanomaterials for efficient electrocatalytic water splitting, Angew. Chem. Int. Ed. 58 (2019) 4484–4502.
[7] J. Huang, Y. Li, Y. Zhang, G. Rao, C. Wu, Y. Hu, X. Wang, R. Lu, Y. Li, J. Xiong, Identification of key reversible intermediates in self-reconstructed nickel-based hybrid electrocatalysts for oxygen evolution, Angew. Chem. Int. Ed. 58 (2019) 17458–17464.
[8] J. Huang, Y. Sun, Y. Zhang, G. Zou, C. Yan, S. Cong, T. Lei, X. Dai, J. Guo, R. Lu, Y. Li, J. Xiong, A new member of electrocatalysts based on nickel metaphosphate nanocrystals for efficient water oxidation, Adv. Mater. (2018) 30.
[9] J. Huang, Y. Sun, X. Du, Y. Zhang, C. Wu, C. Yan, Y. Yan, G. Zou, W. Wu, R. Lu, Y. Li, J. Xiong, Cytomembrane-structure-inspired active Ni-N-O interface for enhanced oxygen evolution reaction, Adv. Mater. (2018) 30.
[10] C. Spoeri, P. Briois, N. Hong Nhan, T. Reier, A. Billard, S. Kuehl, D. Teschner, P. Strasser, Experimental activity descriptors for iridium-based catalysts for the electrochemical oxygen evolution reaction (OER), ACS Catal. 9 (2019) 6653–6663.
[11] H.-S. Oh, H.N. Nong, T. Reier, M. Gliech, P. Strasser, Oxide-supported Ir nanodendrites with high activity and durability for the oxygen evolution reaction in acid PEM water electrolyzers, Chem. Sci. 6 (2015) 3321–3328.
[12] B.M. Tackett, W. Sheng, S. Kattel, S. Yao, B. Yan, K.A. Kuttiyiel, Q. Wu, J.G. Chen, Reducing iridium loading in oxygen evolution reaction electrocatalysts using core-shell particles with nitride cores, ACS Catal. 8 (2018) 2615.
[13] J. Lim, D. Park, S.S. Jeon, C.-W. Roh, J. Choi, D. Yoon, M. Park, H. Jung, H. Lee, Ultrathin IrO2 nanoneedles for electrochemical water oxidation, Adv. Funct. Mater. 28 (2018).
[14] C. Koenigsmann, S.S. Wong, One-dimensional noble metal electrocatalysts: a promising structural paradigm for direct methanol fuel cells, Energy Environ. Sci. 4 (2011) 1161–1176.
[15] Y. Kim, J.G. Kim, Y. Noh, W.B. Kim, An overview of one-dimensional metal nanostructures for electrocatalysis, Catal. Surv. Asia 19 (2015) 88–121.
[16] Q. Shi, C. Zhu, D. Du, J. Wang, H. Xia, M.H. Engelhard, S. Feng, Y. Lin, Ultrathin dendritic IrTe nanotubes for an efficient oxygen evolution reaction in a wide pH range, J. Mater. Chem. 6 (2018) 8855–8859.
[17] S.D. Ghadge, P.P. Patel, M.K. Datta, O.I. Velikokhatnyi, P.M. Shanthi, P.N. Kumta, First report of vertically aligned (Sn,Ir)O-2:F solid solution nanotubes: highly efficient and robust oxygen evolution electrocatalysts for proton exchange membrane based water electrolysis, J. Power Sources 392 (2018) 139–149.
[18] A. Yu, C. Lee, M.H. Kim, Y. Lee, Nanotubular iridium-cobalt mixed oxide crystalline architectures inherited from cobalt oxide for highly efficient oxygen evolution reaction catalysis, ACS Appl. Mater. Interfaces 9 (2017) 35057–35066.
[19] J.H. Shim, Y. Lee, M. Kang, J. Lee, J.M. Baik, Y. Lee, C. Lee, M.H. Kim, Hierarchically driven IrO2 nanowire electrocatalysts for direct sensing of biomolecules, Anal. Chem. 84 (2012) 3827–3832.
[20] C. Wang, M. Waje, X. Wang, J.M. Tang, R.C. Haddon, Y.S. Yan, Proton exchange membrane fuel cells with carbon nanotube based electrodes, Nano Lett. 4 (2004) 345–348.
[21] D.C. Higgins, D. Meza, Z. Chen, Nitrogen-doped carbon nanotubes as platinum catalyst supports for oxygen reduction reaction in proton exchange membrane fuel cells, J. Phys. Chem. C 114 (2010) 21982–21988.
[22] H. Yoo, K. Oh, Y.R. Lee, K.H. Row, G. Lee, J. Choi, Simultaneous co-doping of RuO2 and IrO2 into anodic TiO2 nanotubes: a binary catalyst for electrochemical water splitting, Int. J. Hydrogen Energy 42 (2017) 6657–6664.
[23] W.-H. Ryu, Y.W. Lee, Y.S. Nam, D.-Y. Youn, C.B. Park, I.-D. Kim, Crystalline IrO2-decorated TiO2 nanofiber scaffolds for robust and sustainable solar water oxidation, J. Mater. Chem. 2 (2014) 5610–5615.
[24] L. Zhang, Z.-G. Shao, H. Yu, X. Wang, B. Yi, IrO2 coated TiO2 nanopore arrays electrode for SPE HBr electrolysis, J. Electroanal. Chem. 688 (2013) 262–268.
[25] R. Shan, Z. Zhang, M. Kan, T. Zhang, Q. Zan, Y. Zhao, A novel highly active nanostructured IrO2/Ti anode for water oxidation, Int. J. Hydrogen Energy 40 (2015) 14279–14283.
[26] W. Hu, S. Chen, Q. Xia, IrO2/Nb-TiO2 electrocatalyst for oxygen evolution reaction in acidic medium, Int. J. Hydrogen Energy 39 (2014) 6967–6976.
[27] G. Liu, J. Xu, Y. Wang, X. Wang, An oxygen evolution catalyst on an antimony doped tin oxide nanowire structured support for proton exchange membrane liquid water electrolysis, J. Mater. Chem. 3 (2015) 20791–20800.
[28] V. Avila-Vazquez, M. Galvan-Valencia, J. Ledesma-Garcia, L.G. Arriaga, V.H. Collins-Martinez, C. Guzman-Martinez, I.L. Escalante-Garcia, S.M. Duron-Torres, Electrochemical performance of a Sb-doped SnO2 support synthesized by coprecipitation for oxygen reactions, J. Appl. Electrochem. 45 (2015) 1175–1185.
[29] A.T. Marshall, R.G. Haverkamp, Electrocatalytic activity of IrO2-RuO2 supported on Sb-doped SnO2 nanoparticles, Electrochim. Acta 55 (2010) 1978–1984.
[30] Z.-X. Lu, Y. Shi, C.-F. Yan, C.-Q. Guo, Z.-D. Wang, Investigation on IrO2 supported on hydrogenated TiO2 nanotube array as OER electro-catalyst for water electrolysis, Int. J. Hydrogen Energy 42 (2017) 3572–3578.
[31] Y. Shi, Z. Lu, L. Guo, Z. Wang, C. Guo, H. Tan, C. Yan, Fabrication of IrO2 decorated vertical aligned self-doped TiO2 nanotube arrays for oxygen

evolution in water electrolysis, Int. J. Hydrogen Energy 43 (2018) 9133–9143.
[32] C. Zhao, H. Yu, Y. Li, X. Li, L. Ding, L. Fan, Electrochemical controlled synthesis and characterization of well-aligned IrO2 nanotube arrays with enhanced electrocatalytic activity toward oxygen evolution reaction, J. Electroanal. Chem. 688 (2013) 269–274.
[33] E. Mafakheri, A. Salimi, R. Hallaj, A. Ramazani, M.A. Kashi, Synthesis of iridium oxide nanotubes by electrodeposition into polycarbonate template: fabrication of Chromium(III) and arsenic(III) electrochemical sensor, Electroanalysis 23 (2011) 2429–2437.
[34] M. Cerro-Lopez, Y. Meas-Vong, M.A. Mendez-Rojas, C.A. Martinez-Huitle, M.A. Quiroz, Formation and growth of PbO2 inside TiO2 nanotubes for environmental applications, Appl. Catal. B Environ. 144 (2014) 174–181.
[35] J.M. Macak, B.G. Gong, M. Hueppe, P. Schmuki, Filling of TiO2 nanotubes by self-doping and electrodeposition, Adv. Mater. 19 (2007) 3027.
[36] Q. Wang, K. Zhu, N.R. Neale, A.J. Frank, Constructing ordered sensitized heterojunctions: bottom-up electrochemical synthesis of p-type semiconductors in oriented n-TiO2 nanotube Arrays, Nano Lett. 9 (2009) 806–813.
[37] B.-S. Lee, S.H. Ahn, H.-Y. Park, I. Choi, S.J. Yoo, H.-J. Kim, D. Henkensmeier, J.Y. Kim, S. Park, S.W. Nam, K.-Y. Lee, J.H. Jang, Development of electrodeposited IrO2 electrodes as anodes in polymer electrolyte membrane water electrolysis, Appl. Catal. B Environ. 179 (2015) 285–291.
[38] K. Yamanaka, Anodically electrodeposited iridium oxide-films (aeirof) from alkaline-solutions for electrochromic display devices, Japan. J. Appl. Phys. Part 1-Reg. Pap. Short Notes Rev. Pap. 28 (1989) 632–637.
[39] Y. Zhang, M. Cao, H. Lv, J. Wei, Y. Gu, D. Liu, W. Zhang, M.P. Ryan, X. Wu, Electrodeposited nanometer-size IrO2/Ti electrodes with 0.3 mg IrO2 cm(-2) for sludge dewatering electrolysers, Electrochim. Acta 265 (2018) 507–513.
[40] M. Graf, J. Poppe, A. Eychmueller, Surface influences on the electrodiffusive behavior in mesoporous templates, Small 11 (2015) 3174–3182.
[41] N. Tasaltin, S. Ozturk, N. Kilinc, H. Yuzer, Z.Z. Ozturk, Fabrication of Pd-Fe nanowires with a high aspect ratio by AAO template-assisted electrodeposition, J. Alloys Compd. 509 (2011) 3894–3898.
[42] T. Reier, H.N. Nong, D. Teschner, R. Schloegl, P. Strasser, Electrocatalytic oxygen evolution reaction in acidic environments - reaction mechanisms and catalysts, Adv. Energy Mater. 7 (2017).
[43] J. Cheng, J. Yang, S. Kitano, G. Juhasz, M. Higashi, M. Sadakiyo, K. Kato, S. Yoshioka, T. Sugiyama, M. Yamauchi, N. Nakashima, Impact of Ir-valence control and surface nanostructure on oxygen evolution reaction over a highly efficient Ir-TiO2 nanorod catalyst, ACS Catal. 9 (2019) 6974–6986.
[44] J.J. Conde, A.M. Chaparro, P. Ferreira-Aparicio, Understanding the behavior of electrosprayed carbon black-nafion composite layers, Fuel Cell. 18 (2018) 627–639.
[45] S.M. Andersen, R. Dhiman, E. Skou, X-ray photoelectron spectroscopy investigation on electrochemical degradation of proton exchange membrane fuel cell electrodes, J. Power Sources 282 (2015) 87–94.
[46] T. Reier, Z. Pawolek, S. Cherevko, M. Bruns, T. Jones, D. Teschner, S. Selve, A. Bergmann, H.N. Nong, R. Schlogl, K.J.J. Mayrhofer, P. Strasser, Molecular insight in structure and activity of highly efficient, low-Ir Ir-Ni oxide catalysts for electrochemical water splitting (OER), J. Am. Chem. Soc. 137 (2015) 13031–13040.
[47] S.H. Lee, J. Kim, D.Y. Chung, J.M. Yoo, H.S. Lee, M.J. Kim, B.S. Mun, S.G. Kwon, Y.-E. Sung, T. Hyeon, Design principle of Fe-N-C electrocatalysts: how to optimize multimodal porous structures? J. Am. Chem. Soc. 141 (2019) 2035–2045.
[48] P.L. Taberna, P. Simon, J.F. Fauvarque, Electrochemical characteristics and impedance spectroscopy studies of carbon-carbon supercapacitors, J. Electrochem. Soc. 150 (2003) A292–A300.
[49] H. Shin, H.-i. Kim, D.Y. Chung, J.M. Yoo, S. Weon, W. Choi, Y.-E. Sung, Scaffold-like titanium nitride nanotubes with a highly conductive porous architecture as a nanoparticle catalyst support for oxygen reduction, ACS Catal. 6 (2016) 3914–3920.
[50] M.A. Petit, V. Plichon, Anodic electrodeposition of iridium oxide films, J. Electroanal. Chem. 444 (1998) 247–252.
[51] A.W. Jensen, G.W. Sievers, K.D. Jensen, J. Quinson, J.A. Arminio-Ravelo, V. Brueser, M. Arenz, M. Escudero-Escribano, Self-supported nanostructured iridium-based networks as highly active electrocatalysts for oxygen evolution in acidic media, J. Mater. Chem. 8 (2020) 1066–1071.
[52] Z. Chen, M. Waje, W. Li, Y. Yan, Supportless Pt and PtPd nanotubes as electrocatalysts for oxygen-reduction reactions, Angew. Chem. Int. Ed. 46 (2007) 4060–4063.